Title

Tailoring Metal-Porphyrin-Like Active Sites on Graphene to Improve the Efficiency and Selectivity of Electrochemical CO2 Reduction

Journal

The Journal of Physical Chemistry C, 119(37)

ISSN

1932-7447

Authors

Cheng, Mu-Jeng
Kwon, Youngkook
Head-Gordon, Martin
et al.

Publication Date

2015-09-17

DOI

10.1021/acs.jpcc.5b05518

Peer reviewed

THE JOURNAL OF PHYSICAL CHEMISTRY C

Article

pubs.acs.org/JPCC

Tailoring Metal-Porphyrin-Like Active Sites on Graphene to Improve the Efficiency and Selectivity of Electrochemical CO_2 Reduction

Mu-Jeng Cheng,[†,‡] Youngkook Kwon,[†,‡] Martin Head-Gordon,[*,†,§] and Alexis T. Bell[*,†,‡]

[†]The Joint Center for Artificial Photosynthesis, Lawrence Berkeley National Laboratory, 1 Cyclotron Road, Berkeley, California 94720, United States

[‡]Department of Chemical and Biomolecular Engineering, University of California at Berkeley, 107 Gilman Hall, Berkeley, California 94720, United States

[§]Department of Chemistry, University of California at Berkeley, 419 Latimer Hall, Berkeley, California 94720, United States

Supporting Information

ABSTRACT: Density functional theory (DFT) calculations are performed to investigate the energetics of the CO_2 electrochemical reduction on metal (M) porphyrin-like motifs incorporated into graphene layers. The objective is to develop strategies that enhance CO_2 reduction while suppressing the competitive hydrogen evolution reaction (HER). We find that there exists a scaling relation between the binding energy of the catalyst to hydrogen and that to COOH, a key intermediate in the reduction of CO_2 to CO; however, the M−H bond is stronger than the M−COOH bond, driving the reaction toward the HER rather than the reduction of CO_2 to CO. This scaling relation holds even with axial ligation to the metal cation coordinated to the porphyrin ring. When 4f lanthanide or 5f actinide elements are used as the reactive center, the scaling relation still holds but the M−COOH bond is stronger than the M−H bond, and the reaction favors the reduction of CO_2 to CO. By contrast, there is no scaling relation between the binding energy of the catalyst to H and that to OCHO, the key intermediate in CO_2 reduction to formic acid. Interestingly, we find that coordination of a ligand to an unoccupied axial site can make the M−OCHO bond stronger than the M−H bond, resulting in preferential formic acid formation. This means that the axial ligand effectively enhances CO_2 reduction to formic acid and suppresses the HER. Our DFT calculations have also identified several promising electrocatalysts for CO_2 reduction to HCOOH with almost zero overpotentials.

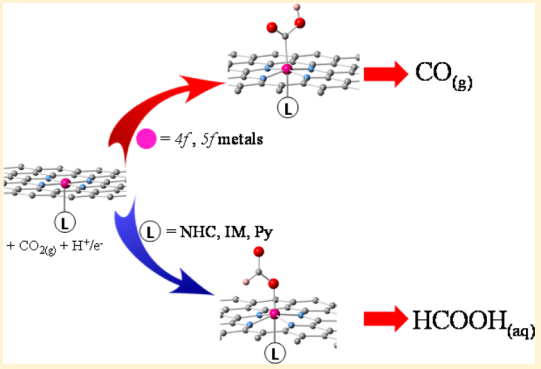

1. INTRODUCTION

One of the grand challenges in modern science and technology is the development of an artificial photosynthesis process that reduces CO_2 and stores the energy in the form of chemical bonds.[1,2] This process requires electrocatalysts that are active, highly selective, inexpensive, and stable. Currently, copper and its alloys are the only catalysts capable of producing significant quantities of hydrocarbons from CO_2; however, these reactions require overpotentials in excess of 1 V.[3−6] A further challenge is to identify catalyst that promotes the CO_2 reduction reaction (CO_2RR) rather than the hydrogen evolution reaction (HER).[4] Therefore, there is a need to develop strategies for suppressing the HER relative to the CO_2RR.

In this study, we have used density functional theory (DFT) to develop strategies for enhancing the CO_2RR and suppressing the HER. For this effort we considered a novel class of electrocatalysts consisting of a metal atom coordinated to a porphyrin ring embedded in graphene. This type of catalyst is chosen for several reasons. N_4 macrocyclic complexes, such as porphyrins,[7−9] corroles,[10] and phthalocyanines,[11−14] are known as electrocatalysts for the CO_2RR. For example, it has been shown by Savéant et al. that iron 5,10,15,20-tetrakis(2′,6′-dimethoxyphenyl)-porphyrin is capable of electrochemical conversion of CO_2 to CO with high Faradaic yield (>90%) and high turnovers (∼50 million) at low overpotentials (0.465 V).[7] Cobalt and nickel phthalocyanines deposited on carbon electrodes have been found to catalyze the electroreduction of CO_2 to formic acid in acid solutions (pH 3−7), and they are also capable of reducing CO_2 to methanol at pH <4, although the current efficiency is <5%.[13] Second, graphene[15,16] and carbon nanotubes[17,18] into which Fe-porphyrin-like motifs are embedded have been reported to be excellent electrocatalysts for the oxygen reduction reaction (ORR). For example, Lee et al. have synthesized carbon nanotubes incorporating porphyrin Fe−N_4 moieties and found that they exhibit excellent ORR catalytic activity as well as high structural stability over 10^6 cycles.[17] More recently it has been reported that nitrogen-doped carbon nanotubes are selective and robust electrocatalysts for CO_2 reduction to formic acid.[19] The third key reason for selecting metal-porphyrin-functionalized graphene as

Received: June 9, 2015
Revised: August 20, 2015
Published: August 24, 2015

DOI: 10.1021/acs.jpcc.5b05518
J. Phys. Chem. C 2015, 119, 21345−21352

catlayts motif is that the activity of the site can be tuned by changing the central metal (**M**) and through the choice of ligand (**L**) coordinated to the vacant axial site. It should be noted that, in addition to these N_4 macrocyclic complexes, there exist several metallic electrocatalysts (e.g., Au, Ag, and PtPd alloys) that exhibit low overpotentials and high Faradaic efficiencies for CO_2 reduction to CO[20,21] or HCOOH.[22]

In this study, we only considered two-proton−two-electron ($2H^+/2e^-$) CO_2 reduction reactions, namely, CO_2 reduction to carbon monoxide (CO) and formic acid (HCOOH), and compared the energetics to those for the HER. These processes together with the equilibrium potential at pH 0 for each are shown in Scheme 1, and an illustration of the progress of these

Scheme 1. HER and Two $2H^+/2e^-$ CO_2RR Reactions[a]

$$2H^+ + 2e^- \longrightarrow H_2 \qquad U = 0.0\ V$$

$$CO_2 + 2H^+ + 2e^- \longrightarrow CO + H_2O \qquad U = -0.12\ V$$

$$CO_2 + 2H^+ + 2e^- \longrightarrow HCOOH_{(aq)} \qquad U = -0.20\ V$$

[a]Corresponding equilibrium potential for each reaction is indicated.

processes on metal-porphyrin-functionalized graphene (**G-Por-M(L)**, **M** = Ni^{2+}, Co^{2+}, Fe^{2+}, Mn^{2+}, and Cr and **L** = **Py**, **IM**, and **NHC**) is shown in Scheme 2.

We consider the metal-porphyrin-functionalized graphene (**G-Por-M(L)**, **M** = Ni^{2+}, Co^{2+}, Fe^{2+}, Mn^{2+}, and Cr^{2+} and **L** = **Py**, **IM** and **NHC**) to consist of isolated active sites. As a result, the competition between the initial intermediates involved in the three target reactions (*H, *COOH, and *OCHO) for those active sites determines the fate of the electrocatalysis.[23,24] For example, if an active site is first occupied by *H as the applied voltage becomes more negative, then the HER would be the primary pathway and the CO_2RR would be minimized. Because the formation of those intermediates involves the transfer of one H^+/e^-, the related stability of the *H, *COOH, and *OCHO intermediates is not affected by the change of the applied voltage or pH. As a consequence, the key to suppressing the HER and enhancing the CO_2RR is to develop strategies that strengthen the binding between the active sites and COOH (or OCHO) while weakening the interaction between those sites and H, leading to the requirement that $\Delta G_{*COOH} < \Delta G_{*H}$ or $\Delta G_{*OCOH} < \Delta G_{*H}$. The goal of this paper is to show how this can be achieved.

The remainder of this paper is organized as follows. In Section 2, the density functional theory (DFT) methods used to perform our calculations are described. Our results are described in Section 3, beginning in Section 3.1 with a discussion of the role that active site composition (choice of **M**, **L**) has on the competition between the HER and the *COOH branch of the CO_2RR that yields CO (the gateway toward methanol, methane, etc.). It will be shown that the class of metal used (transition metal versus rare-earth metal) dictates the selectivity, while the choice of axial ligand is relatively inconsequential. In Section 3.2, we consider the additional issue of selectivity between HER and CO_2RR to yield CO and the other possible branch of the CO_2RR to yield formic acid, HCOOH, via the *OCHO intermediate. Selectivity toward formic acid production can be tuned by the choice of axial ligand. Finally, in Section 3.3, we consider the extent to which the overpotential for formic acid production can be minimized within the active-site paradigm studied here, and we show that very low overpotentials appear to be achievable.

2. COMPUTATIONAL DETAILS

DFT calculations were performed using the Vienna ab initio Simulation Package (VASP)[25−28] with the projector augmented wave pseudopotentials[29,30] and the PBE functional.[31] The plane wave energy cutoff was set to 400 eV, and electron smearing was employed using the Gaussian-smearing technique with a width of k_BT = 0.1 eV for the graphene systems and 0.01 eV for

Scheme 2. Three Two-Proton-Electron-Pair Reduction Pathways Considered in This Study[a]

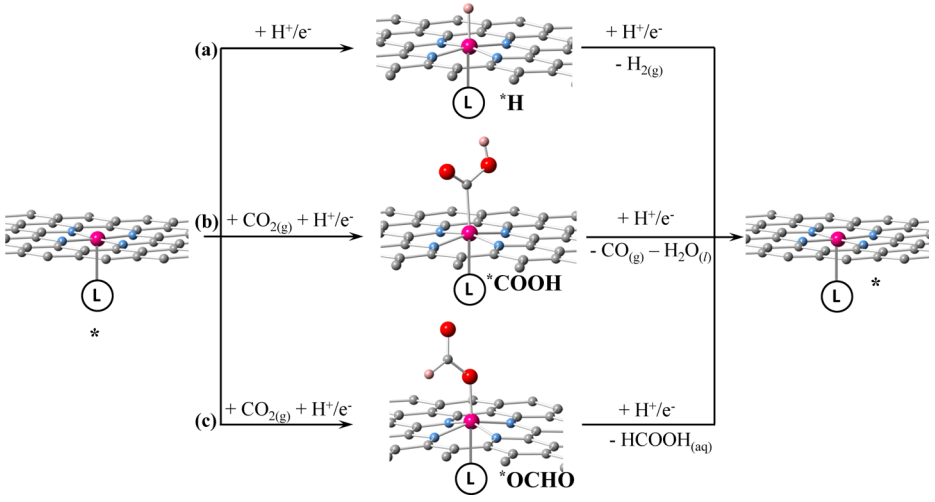

[a]The asterisk indicates a species coordinated to the metal cation. **L** represents an axial ligand. It should be noted that in our model the concentration of active sites is one Fe−N_4 per 26 carbon atoms, which is almost four times higher than that in the experimental work reported in ref 17 (one Fe−N_4 per 100 carbon atoms); however, because the active sites in our model are highly isolated (the distance between two adjacent active sites is at least 8.5 Å), we do not expect a significant change in the Gibbs free-energy surfaces if the concentration of active sites was lowered to the level reported in experimental studies. Regarding the orientation of O−H in *COOH, it is energetically more favorable for the O−H to point away from (as depicted in the scheme) rather than towards the graphene surface.

DOI: 10.1021/acs.jpcc.5b05518
J. Phys. Chem. C 2015, 119, 21345−21352

Table 1. Calculated Energetics for *H (ΔG_{*H}), *COOH (ΔG_{*COOH}), *OCHO (ΔG_{*OCHO}), and the Overpotentials Required for the Formation of H_2 (η^{H2}), CO (η^{CO}), and HCOOH (η^{HCOOH})[a]

catalyst	ΔG_{*H}	η^{H2}	ΔG_{*COOH}	η^{CO}	ΔG_{*OCHO}	η^{HCOOH}
G-Por-Ni	1.75	1.75	1.85	1.73	**1.36**	**1.17**
G-Por-Co	**0.18**	**0.18**	0.35	0.23	0.64	0.46
G-Por-Fe	**0.19**	**0.19**	0.34	0.22	0.35	0.17
G-Por-Mn	**0.39**	**0.39**	0.52	0.40	0.39	0.21
G-Por-Cr	0.14	0.14	0.21	0.09	**−0.37**	**0.55**
G-Por-Ni(Py)	1.62	1.62	1.85	1.73	**1.28**	1.10
G-Por-Co(Py)	**0.21**	0.21	0.48	0.36	0.49	0.30
G-Por-Fe(Py)	0.40	0.40	0.60	0.48	**0.32**	0.13
G-Por-Mn(Py)	0.43	0.43	0.63	0.51	**0.23**	0.05
G-Por-Cr(Py)	0.57	0.57	0.71	0.59	**−0.09**	0.27
G-Por-Ni(IM)	1.57	1.57	1.84	1.72	**1.28**	1.09
G-Por-Co(IM)	**0.22**	0.22	0.47	0.35	0.39	0.20
G-Por-Fe(IM)	0.38	0.38	0.53	0.41	**0.21**	0.02
G-Por-Mn(IM)	0.42	0.42	0.59	0.47	**0.16**	0.03
G-Por-Cr(IM)	0.53	0.53	0.65	0.53	**−0.20**	0.38
G-Por-Ni(NHC)	1.10	1.10	1.46	1.34	**1.02**	**0.84**
G-Por-Co(NHC)	0.33	0.33	0.53	0.41	**−0.01**	**0.19**
G-Por-Fe(NHC)	0.95	0.95	1.06	0.94	**0.43**	**0.24**
G-Por-Mn(NHC)	0.52	0.52	0.65	0.53	**−0.07**	**0.26**
G-Por-Cr(NHC)	0.94	0.94	1.03	0.91	**0.03**	**0.15**
Ac-Ni	1.70	1.70	1.68	1.56	**1.56**	**1.37**
Ac-Co	**0.36**	**0.36**	0.43	0.31	0.94	0.76
Ac-Fe	0.53	0.53	0.56	0.44	**0.38**	**0.19**
Ac-Mn	0.55	0.55	0.59	0.47	**0.36**	**0.18**
Ac-Cr	0.46	0.46	0.55	0.43	**−0.06**	**0.24**
Ac-Th	−0.62	0.62	−0.93	1.05	**−2.18**	**2.36**
Ac-Pa	−0.61	0.61	−0.89	1.01	**−2.17**	**2.36**
Ac-U	−0.24	0.24	−0.68	0.80	**−1.89**	**2.07**
Ac-Cm	−0.32	0.32	−0.55	0.67	**−1.84**	**2.02**
Ac-Ce	0.27	0.27	−0.22	0.34	**−1.48**	**1.66**
Ac-Pr	0.38	0.38	−0.10	0.22	**−1.36**	**1.54**

[a]Units are electronvolts for energetics and volts for overpotentials.

molecules. All calculated values of energy were extrapolated to $k_BT = 0$. For the graphene systems, a Monkhorst−Pack k-point grid of 2 × 2 × 1 was chosen to sample the reciprocal space, whereas for molecules only the gamma point was sampled. For graphene, at least 10 Å vacuum space between adjacent images was used to prevent the interaction between the replicas along the z direction, while for all molecules, a 20 Å × 20 Å × 20 Å box was used for simulations. Spin-polarized wave functions were used for all calculations except H_2, CO, HCOOH, and CO_2. All possible spin states for each system were calculated by constraining the difference between the numbers of α and β electrons ranging from 0 to 8, but only the most stable one was used for discussion.

Zero-point energy (ZPE), enthalpic, and entropic corrections and solvation energies are needed to convert electronic energies into Gibbs free energies. For graphene and organometallic systems, ZPE and thermodynamic corrections were taken as the numbers calculated for the **G-Por-Mn** system based on the finite difference method. Solvation corrections were calculated for each system using the Poisson−Boltzmann implicit solvation model[32,33] with a dielectric constant $\varepsilon = 80$ for water. By contrast, the solvation energies for $H_2O_{(l)}$ and $HCOOH_{(aq)}$ were calculated by using their vapor pressure at 1 atm (3534 Pa for H_2O and 2 Pa for HCOOH).

Only concerted proton−electron transfer was considered because the materials studied here are metallic based on their DOS. The computational standard hydrogen electrode model proposed by Nørskov and coworkers was used to calculate potential- and pH-dependent free-energy surfaces.[34] In the context of this model, the free energy of a proton and an electron is equal to half the free energy of $H_{2(g)}$ at an applied electric potential U = 0 V versus SHE and pH 0. The overpotential (η) is estimated as the difference between the equilibrium potential and the least-negative applied potential at which each step on the pathway becomes exergonic. (See an example in the Supporting Information.) It should be noted that we only considered thermodynamics and ignored kinetics to obtain our estimates of η. We, therefore, assume that the barriers for electrochemical proton transfers are small and easily surmountable at room temperature. In fact, it has been shown computationally that the proton-transfer barriers for oxygen reduction reaction on Pt surfaces are small (0.15 to 0.25 eV) and diminished at higher applied voltages.[35,36]

3. RESULTS AND DISCUSSION

3.1. Hydrogen Evolution versus CO_2 to CO Reduction (Competition between *H and *COOH). Table 1 lists the calculated Gibbs free energies of the three intermediates (ΔG_{*H}, ΔG_{*COOH}, ΔG_{*OCHO}), referenced to the energies of proton and electron pairs (at pH 0 and U = 0 V) and $CO_{2(g)}$ (P = 1 atm) and their corresponding overpotentials for $H_{2(g)}$, $CO_{(g)}$, and $HCOOH_{(aq)}$ formation (η^{H2}, η^{CO}, η^{HCOOH}). The

DOI: 10.1021/acs.jpcc.5b05518
J. Phys. Chem. C 2015, 119, 21345−21352

data in Table 1 includes a range of **G-Por-M(L)** active sites, corresponding to abundant first-row transition metals, with and without axial ligands, **L**, as well as some rare-earth elements. This large amount of computational data will be analyzed in the remainder of this subsection, as well as the following subsections.

We first compared ΔG_{*H} and ΔG_{*COOH} to identify the conditions under which $\Delta G_{*COOH} < \Delta G_{*H}$ and therefore the reduction of CO_2 to CO should be favored over the evolution of H_2. Figure 1 summarizes these data for the transition metals

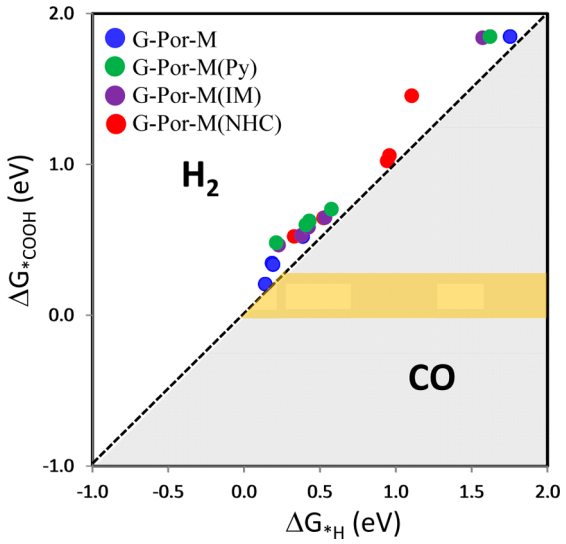

Figure 1. Scaling relation between ΔG_{*H} and ΔG_{*COOH} for transition-metal ions, M, in a **G-Por-M(L)** (**L** = **Py**, **IM**, **NHC**) active site. In the gray shaded area, $\Delta G_{*COOH} < \Delta G_{*H}$; therefore, CO_2 reduction to CO is more favorable than H_2 evolution. In the orange shaded area, the overpotential, η^{CO}, is minimized. While a very good scaling relation is evident, no viable catalysts for selective CO_2 reduction to CO emerge from this data (also shown in tabular form in Table 1).

and reveals that there is a good linear correlation between ΔG_{*COOH} and ΔG_{*H} for all of the **G-Por-M** sites; however, for all transition metals, $\Delta G_{*COOH} > \Delta G_{*H}$, and correspondingly $\eta^{H2} < \eta^{CO}$. This means that for all of the catalysts considered the HER would dominate over the CO_2RR. The same trend has been reported by Tripkovic et al. for the same system[24] and also for some binary alloys.[23]

Recently, we have found that axial coordination of a ligand to an Fe-porphyrin group incorporated into graphene or carbon nanotubes reduces the overpotentials required for the oxygen evolution reaction (OER) and also for the oxygen reduction reaction (ORR) by ~0.3 V.[37] Analysis showed that this is due to stabilization of key intermediates for the ORR and OER by the axial ligand, resulting in a change in the Gibbs free energy surfaces and leading to a reduction in the overpotential for each of these reactions. Consistent with our previous DFT study, recent experiments have indeed found that the use of judiciously chosen axial ligands promotes the ORR activity of tethered iron phthalocyanine carbon nanotube[38] and tethered iron tetraphenylporphyrin graphene.[39]

We, therefore, applied the same approach here to determine whether axial ligands would bind with *COOH more tightly than *H, making *COOH a more favorable intermediate and driving the reaction toward the reduction of CO_2 to CO. As illustrated in Scheme 3a, an N-heterocyclic carbene (**NHC**),

Scheme 3. (a) Axial Ligands Investigated in This Study and (b) Metal Acetylacetonates Complex

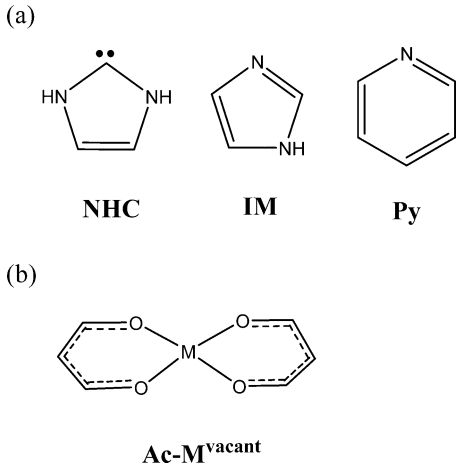

imidazole (**IM**), and pyridine (**Py**) were chosen for investigation. These ligands were chosen because they have been shown both theoretically[37] and experimentally[38,39] to promote activity for the ORR. Table 1 and Figure 1 show, however, that active sites incorporating these ligands, **G-Por-M(L)** (**L** = **Py**, **IM**, **NHC**), still obey the same scaling relation, and ΔG_{*H} remains lower than ΔG_{*COOH}. We conclude that these axial ligands do not change the outcome of electrocatalysis and that the HER remains the more favorable reaction pathway.

The next change in the active site design we considered was the introduction of rare-earth metal cations in place of transition-metal cations. In organometallic chemistry, it is well known that the small binding energy differences between M−H and M−C bonds in actinide alkyl complexes make them less prone to β-hydride elimination than transition-metal elements.[40] This suggests that actinide-centered catalysts may result in $\Delta G_{*COOH} < \Delta G_{*H}$, making CO_2 reduction to CO more favorable than the HER. We evaluated this hypothesis by using 5f actinide cations Th^{2+}, Pa^{2+}, U^{2+}, and Cm^{2+} and also 4f lanthanide cations Ce^{2+} and Pr^{2+} as catalytic centers. The synthesis of 5f actinide and 4f lanthanide metal complexes is well-documented in the literature,[40−43] and some of these complexes have been demonstrated to exhibit activity for the reduction of CO_2.[44−47]

Because of their much larger diameters, these rare-earth metal cations cannot fit in the N_4 pocket of porphyrins. We therefore used a more flexible acetylacetonate ligand (**Ac-M**, **M** = Th^{2+}, Pa^{2+}, U^{2+}, Cm^{2+}, Ce^{2+}, and Pr^{2+}, Scheme 3b) to test the proposed idea. To assess the difference between the acetylacetonate and porphyrin macrocycles, we also repeated the calculations with the same five transition metals previously used. The results are plotted in Figure 2 and are also part of the comprehensive results given in Table 1. The transition-metal **Ac-M** results are very similar to those obtained previously with the **G-Por-M** site, with just a slight shift (~0.1 eV) toward stabilizing ΔG_{*COOH} versus ΔG_{*H}.

By contrast, we find that for complexes involving 4f and 5f metals, ΔG_{*COOH} is significantly lower than ΔG_{*H}. Thus, use of rare-earth cations effectively changes the scaling relation between ΔG_{*COOH} and ΔG_{*H} in favor of the CO pathway. Comparison with the transition-metal results shows that it is

DOI: 10.1021/acs.jpcc.5b05518
J. Phys. Chem. C 2015, 119, 21345−21352

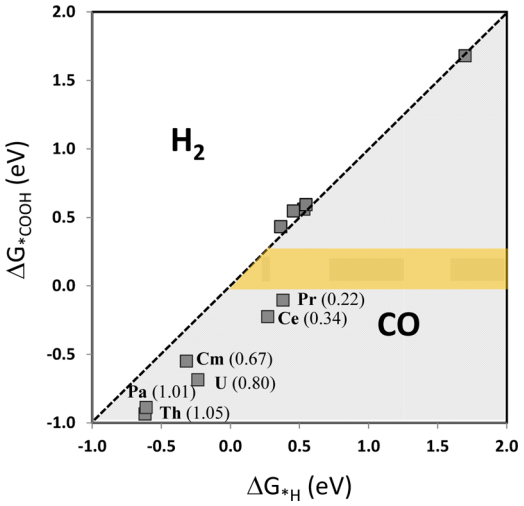

Figure 2. Scaling relation between ΔG_{*H} and ΔG_{*COOH} for transition-metal and rare-earth ions, M, in a **Ac-M** active site. In the gray shaded area, $\Delta G_{*COOH} < \Delta G_{*H}$; therefore, CO_2 reduction to CO is more favorable than H_2 evolution. In the orange shaded area, η^{CO} is minimized. In contrast with the transition metals, the rare earths show good selectivity for CO_2 reduction to CO. Values of η^{CO} are shown in parentheses, with a lowest η^{CO} = 0.22 V.

predominantly the rare-earth metals that cause $\Delta G_{*COOH} < \Delta G_{*H}$ rather than the use of the **Ac** as the ligand.

Further investigation reveals that for the **Ac-M** series, the averaged binding energy difference between M−H and M−CH_3 ($BE_{M-H}-BE_{M-CH3}$, BE is referenced to a vacant site and a hydrogen atom or methyl radical) bonds is 0.31 eV for **M** = Ni^{2+}, Co^{2+}, Fe^{2+}, Mn^{2+}, and Cr^{2+} and is only 0.16 eV for **M** = Th^{2+}, Pa^{2+}, U^{2+}, Cm^{2+}, Ce^{2+}, and Pr^{2+}. This means that moving from the first-row transition metals to the 4f and 5f elements indeed reduces $BE_{M-H}-BE_{M-CH3}$; however, the reduction is only 0.15 eV on average, which is too small to count for the big reduction in $\Delta G_{*COOH} - \Delta G_{*H}$ (average value of 0.41 eV, comparing rare earths vs transition metals at the **Ac-M** sites).

Therefore, there must also be another factor contributing to the observed $\Delta G_{*COOH} < \Delta G_{*H}$ for the complexes involving 4f and 5f elements. Analysis of the structures of the *COOH intermediates shows that for the 4f and 5f complexes, the bond length between metal and oxo of COOH is smaller (R_{M-O} = 2.35−2.45 Å, red dashed line, Scheme 4a) than the Ni, Co, Fe, Mn, and Cr cases (2.90−2.74 Å). For example, for **Ac−Th** and **Ac−Pa**, the values of R_{M-O} are only 2.45 and 2.40 Å, respectively. This indicates that there is an additional orbital interaction between those metals and the O atom that stabilizes the *COOH intermediate and makes the reduction of CO_2 to CO more favorable than the HER. This interaction can be seen from the electron density of one of the highest occupied molecular orbital of **Ac−Th** (Scheme 4b). To evaluate the reliability of the PBE/PAW computational model, we changed the functional to the HSE and separately increased the plane-wave kinetic cutoff to 500 eV in the calculation done for Ac−Ce, Ac−U, and Ac−Th. We find that the results are similar to those based on the PBE/PAW with a 400 eV cutoff (Table S2 in the Supporting Information).

3.2. Hydrogen Evolution versus CO_2 Reduction to Formic Acid. We consider next the problem of selective reduction of $CO_{2(g)}$ to $HCOOH_{(aq)}$ versus proton reduction to $H_{2(g)}$. The criterion for preferential reduction of CO_2 to HCOOH versus the evolution of H_2 is that $\Delta G_{*OCHO} < \Delta G_{*H}$.

Scheme 4. (a) Optimized Structures of the *COOH Intermediates for Ac-M, M = Th^{2+}, Pa^{2+}, U^{2+}, Cm^{2+}, Ce^{2+}, and Pr^{2+} and (b) the Electron Density of One of the Highest Occupied Molecular Orbital of *COOH of Ac−Th

(a)

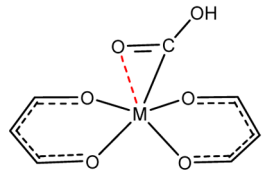

M = Th^{2+}, Pa^{2+}, U^{2+}, Cm^{2+}, Ce^{2+}, and Pr^{2+}

(b)

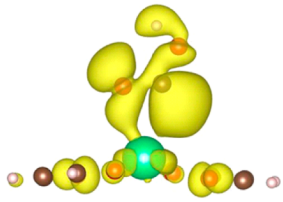

The pathway for the reduction of CO_2 to HCOOH has often not been considered in previous DFT studies,[23,24,48] even though formic acid is a common product of CO_2 reduction.[49] In contrast with the nearly linear relation observed between ΔG_{*H} and ΔG_{*COOH} (see Figure 1), we find that there is a much weaker scaling relation between ΔG_{*H} and ΔG_{*OCHO}, as can be seen from Figure 3. This is not surprising because

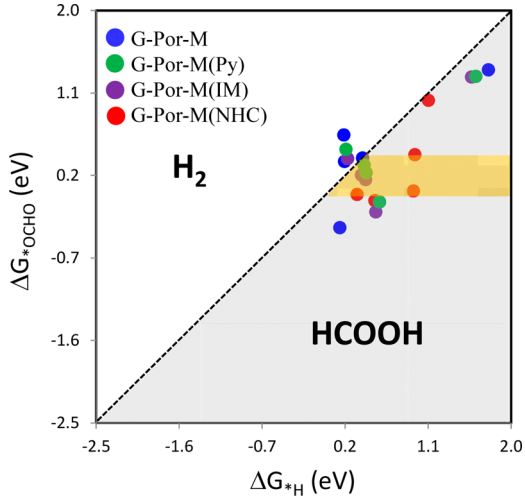

Figure 3. Scaling relation between ΔG_{*H} and ΔG_{*OCHO}. In the gray shaded area, $\Delta G_{*OCHO} < \Delta G_{*H}$; therefore CO_2 reduction to formic acid is more favorable than the H_2 evolution. In the orange shaded area, the η^{HCOOH} is minimized.

OCHO interacts with metals differently than do H and COOH. In addition to having an M−O σ interaction with metals, due to the lone pairs of electrons on O, OCHO also has a π interaction with metals, which is absent in M−H and M−COOH.

Axial ligation of **Py**, **IM**, and **NHC** with the metal has a significant effect on the reduction of CO_2 to HCOOH, making ΔG_{*OCHO} even smaller than ΔG_{*H}. The average value of $(\Delta G_{*OCHO} - \Delta G_{*H})$ decreases from −0.06 eV for **G-Por-M**, to −0.20 eV for **G-Por-M(Py)**, to −0.26 eV for **G-Por-M(IM)**,

DOI: 10.1021/acs.jpcc.5b05518
J. Phys. Chem. C 2015, 119, 21345−21352

and to −0.49 eV for **G-Por-M(NHC)**. In contrast with the **G-Por-M** series of complexes, ΔG_{*OCHO} is lower than ΔG_{*H} for the **G-Por-M(L)** (**L** = **Py**, **IM**, **NHC**) series, with the exception of only **G-Por-Co(IM)** and **G-Por-Co(Py)**. This means that in the presence of axial ligands, particularly **NHC**, *OCHO forms at much less negative applied potentials than *H, and reaction is driven toward HCOOH formation rather than H_2.

The higher stability of *OCHO relative to *H can be explained by the axial ligand stabilization energy (Table 2). All

Table 2. Stabilization Energies for *, *H, *COOH, and *OCHO Intermediate States by the Axial Ligands[a,b]

A\M	Ni	Co	Fe	Mn	Cr
G-Por-M(Py)					
*	0.10	−0.26	−0.53	−0.35	−0.68
*H	−0.03	−0.23	−0.31	−0.32	−0.25
*COOH	0.11	−0.12	−0.26	−0.25	−0.18
*OCHO	0.03	−0.41	−0.56	−0.52	−0.40
G-Por-M(IM)					
*	0.13	−0.27	−0.51	0.23	−0.69
*H	−0.05	−0.23	−0.32	0.37	−0.30
*COOH	0.13	−0.15	−0.31	0.36	−0.24
*OCHO	0.05	−0.53	−0.65	−0.23	−0.52
G-Por-M(NHC)					
*	0.15	−0.77	−1.49	−1.41	−1.37
*H	−0.50	−0.62	−0.72	−1.38	−0.57
*COOH	−0.24	−0.59	−0.76	−1.35	−0.55
*OCHO	−0.18	−1.42	−1.41	−1.65	−0.97

[a]

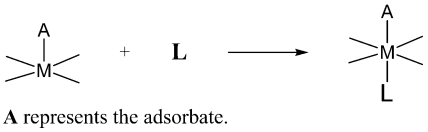

A represents the adsorbate.

A represents the adsorbate. [b]Only electronic energies and solvation energies are considered (ΔE_{elec} + ΔG_{Solv}). The unit for energy is electronvolts.

systems except those containing Ni, **Py**, **IM**, and **NHC** stabilize * and *OCHO intermediates by large and similar amounts (on average, 0.45 and 0.47 eV for **Py**, 0.31 and 0.48 eV for **IM**, and 1.26 and 1.36 eV for **NHC**), while they stabilize *H and *COOH by similar but smaller amounts (0.28 and 0.20 eV for **Py**, 0.12 and 0.09 eV for **IM**, and 0.82 and 0.81 eV for **NHC**). The net effect is that the formation of *OCHO becomes more favorable than *H and *COOH. This finding can also be explained from the molecular orbital point of view. H and COOH bind with metals tightly, pushing the empty $3d_{z^2}$ orbital up in energy, making it energetically unfavorable to bind with **Py**, **IM**, and **NHC**, and leading to a lower axial ligand stabilization energy. By contrast, OCHO binds with metal loosely, making $3d_{z^2}$ lower in energy, forming stronger binding with the axial ligands and stabilizing *OCHO.

We observed that unlike the other metal complexes, those containing Ni behave differently. The magnitudes of the axial ligand stabilization energy for the Ni complexes are significantly lower than those for the Co, Fe, Mn, and Cr complexes and in some cases are even positive, meaning that axial ligand binding is endothermic. This is because for these Ni complexes the $3d_{z^2}$ orbitals are either doubly occupied (for the * intermediate) or singly occupied (for the *H, *COOH, and *OCHO intermediates), which results in a repulsive interaction with the incoming axial ligand, thereby significantly reducing the binding stabilization energy.

Because the CO_2RR occurs under strongly reducing conditions, the metallic center may be reduced from its original oxidation state of +2 to +1 or even zero. For this reason, we also calculated the energetics for **G-Por-M^{+1}** (by adding one more electron to **G-Por-M**). These calculations reveal that consistent with the results for **G-Por-M** there is still a strong scaling relation between ΔG_{*H} and ΔG_{*COOH}; however, in contrast with the results for **G-Por-M**, *OCHO becomes relatively more stable than *H and *COOH (i.e., ΔG_{*OCHO} is now lower than ΔG_{*H} and ΔG_{*COOH}, Table 3). This means that reduction of the metallic center from +2 to +1 would make the reduction of CO_2 to HCOOH even more favorable.

Table 3. Calculated Energetics for *H (ΔG_{*H}), *COOH (ΔG_{*COOH}), and *OCHO (ΔG_{*OCHO}) and the Overpotentials Required for the Formation of H_2 (η^{H2}), CO (η^{CO}), and HCOOH (η^{HCOOH}) for G-Por-M^{+1} (M = Ni, Co, Fe, Mn, and Cr)[a]

catalyst	ΔG_{*H}	η^{H2}	ΔG_{*COOH}	η^{CO}	ΔG_{*OCHO}	η^{HCOOH}
G-Por-Ni^{1+}	1.46	1.46	1.50	1.38	**0.56**	**0.38**
G-Por-Co^{1+}	0.79	0.79	0.95	0.83	**0.34**	**0.16**
G-Por-Fe^{1+}	0.14	0.14	0.14	0.02	**0.14**	**0.04**
G-Por-Mn^{1+}	0.23	0.23	0.27	0.15	**-0.56**	**0.74**
G-Por-Cr^{1+}	−0.05	0.05	0.04	0.08	**-0.57**	**0.76**

[a]Unit is electronvolts for energetics and volts for overpotentials.

3.3. Efficient Electrocatalysts for CO_2 Reduction to Formic Acid. Having demonstrated that selective reduction of CO_2 to formic acid is possible in the presence of protons, the final step in analyzing the data of Table 1 is to consider the associated overpotential. Our calculations predict η^{HCOOH} to be very small for **G-Por-Fe(IM)** (0.02 V), **G-Por-Mn(IM)** (0.03 V), and **G-Por-Mn(Py)** (0.05 V) and small for **G-Por-Fe(Py)** (0.13 V), and **G-Por-Cr(NHC)** (0.15 V).

The discovery of an efficient electrocatalyst for converting CO_2 to formic acid is significant. Formic acid is a promising materials for hydrogen storage due to its high volumetric capacity and its ease of handling and its relatively low toxicity, corrosiveness, and flammability.[50−52] Hydrogen stored as formic acid can be released on demand with the help of homogeneous[53,54] or heterogeneous catalysts,[55,56] to produced CO_2 and H_2, and the latter product can be used directly in a fuel cell. Moreover, formic acid can also be used as an ideal replacement of mineral acids such as HCl and H_2SO_4 for steel pickling[57] and because it is biodegradable and therefore is environmentally friendly. Finally, formic acid fuel cells may be of future technological interest.[58]

4. CONCLUSIONS

DFT calculations have been used to explore the nature of the active site required to achieve the electrochemical reduction of CO_2 in preference to proton reduction to generate H_2. As the active site, we have considered transition-metal cations held by a porphyrin group incorporated into graphene (**G-Por-M**) and both transition-metal cations and rare-earth metal cations complexes of acetylacetonate (**Ac-M**). Our main conclusions are as follows.

(1) We find that a scaling relation exists between the Gibbs free energy of H and COOH binding to the metal cation center

DOI: 10.1021/acs.jpcc.5b05518
J. Phys. Chem. C 2015, 119, 21345−21352

in both **G-Por-M** and **Ac-M**; however, the binding of H atoms is stronger than that of COOH species, which drives the reaction toward H_2 generation rather than CO_2 reduction to CO. This scaling relation holds independent of the presence of an axial ligand and nearly independent of the choice of transition metal.

(2) When rare-earth metal cations (either 4f lanthanide or 5f actinides) are used as the reactive centers, the scaling relation still holds, but the catalysts bind more favorably with COOH than with H, resulting selective in CO_2 reduction to CO.

(3) By contrast, no scaling relation is found between the Gibbs free energy of H and OCHO binding to any of the metal complexes examined. Importantly, we find that when an axial ligand is coordinated to the metal site, the binding of OCHO becomes stronger than that of H, leading to formic acid formation. This means that the axial ligand effectively enhances CO_2 reduction to formic acid and suppresses the formation of H_2.

(4) We have also identified several promising electrocatalysts for selective CO_2 reduction to HCOOH with overpotentials approaching zero.

■ ASSOCIATED CONTENT

Ⓢ Supporting Information

The Supporting Information is available free of charge on the ACS Publications website at DOI: 10.1021/acs.jpcc.5b05518.

Additional tables and details regarding computational methods. (PDF)

■ AUTHOR INFORMATION

Corresponding Authors

*M.H.-G.: E-mail: mhg@cchem.berkeley.edu.

*A.T.B.: E-mail: alexbell@berkeley.edu.

Notes

The authors declare no competing financial interest.

■ ACKNOWLEDGMENTS

This material is based on work performed in the Joint Center for Artificial Photosynthesis, a DOE Energy Innovation Hub, supported through the Office of Science of the U.S. Department of Energy under Award Number DE-SC0004993.

■ REFERENCES

(1) Bensaid, S.; Centi, G.; Garrone, E.; Perathoner, S.; Saracco, G. Towards Artificial Leaves for Solar Hydrogen and Fuels from Carbon Dioxide. *ChemSusChem* **2012**, *5*, 500−521.

(2) Lewis, N. S.; Nocera, D. G. Powering the Planet: Chemical Challenges in Solar Energy Utilization. *Proc. Natl. Acad. Sci. U. S. A.* **2006**, *103*, 15729−15735.

(3) Hori, Y.; Kikuchi, K.; Murata, A.; Suzuki, S. Production of Methane and Ethylene in Electrochemical Reduction of Carbon-Dioxide at Copper Electrode in Aqueous Hydrogencarbonate Solution. *Chem. Lett.* **1986**, 897−898.

(4) Hori, Y.; Wakebe, H.; Tsukamoto, T.; Koga, O. Electrocatalytic Process of Co Selectivity in Electrochemical Reduction of CO_2 at Metal-Electrodes in Aqueous-Media. *Electrochim. Acta* **1994**, *39*, 1833−1839.

(5) Watanabe, M.; Shibata, M.; Kato, A.; Azuma, M.; Sakata, T. Design of Alloy Electrocatalysts for CO_2 Reduction 0.3. The Selective and Reversible Reduction of CO_2 on Cu Alloy Electrodes. *J. Electrochem. Soc.* **1991**, *138*, 3382−3389.

(6) Watanabe, M.; Shibata, M.; Katoh, A.; Sakata, T.; Azuma, M. Design of Alloy Electrocatalysts for CO_2 Reduction - Improved Energy Efficiency, Selectivity, and Reaction Rate for the CO_2 Electroreduction on Cu Alloy Electrodes. *J. Electroanal. Chem. Interfacial Electrochem.* **1991**, *305*, 319−328.

(7) Costentin, C.; Drouet, S.; Robert, M.; Saveant, J. M. A Local Proton Source Enhances CO_2 Electroreduction to CO by a Molecular Fe Catalyst. *Science* **2012**, *338*, 90−94.

(8) Costentin, C.; Passard, G.; Robert, M.; Saveant, J. M. Ultraefficient Homogeneous Catalyst for the CO_2-to-CO Electrochemical Conversion. *Proc. Natl. Acad. Sci. U. S. A.* **2014**, *111*, 14990−14994.

(9) Sonoyama, N.; Kirii, M.; Sakata, T. Electrochemical Reduction of CO_2 at Metal-Porphyrin Supported Gas Diffusion Electrodes under High Pressure CO_2. *Electrochem. Commun.* **1999**, *1*, 213−216.

(10) Grodkowski, J.; Neta, P.; Fujita, E.; Mahammed, A.; Simkhovich, L.; Gross, Z. Reduction of Cobalt and Iron Corroles and Catalyzed Reduction of CO_2. *J. Phys. Chem. A* **2002**, *106*, 4772−4778.

(11) Abe, T.; Yoshida, T.; Tokita, S.; Taguchi, F.; Imaya, H.; Kaneko, M. Factors Affecting Selective Electrocatalytic CO_2 Reduction with Cobalt Phthalocyanine Incorporated in a Polyvinylpyridine Membrane Coated on a Graphite Electrode. *J. Electroanal. Chem.* **1996**, *412*, 125−132.

(12) Isaacs, M.; Armijo, F.; Ramirez, G.; Trollund, E.; Biaggio, S. R.; Costamagna, J.; Aguirre, M. J. Electrochemical Reduction of Co2Mediated by Poly-M-Aminophthalocyanines (M = Co, Ni, Fe): Poly-Co-Tetraaminophthalocyanine, a Selective Catalyst. *J. Mol. Catal. A: Chem.* **2005**, *229*, 249−257.

(13) Kapusta, S.; Hackerman, N. Carbon-Dioxide Reduction at a Metal Phthalocyanine Catalyzed Carbon Electrode. *J. Electrochem. Soc.* **1984**, *131*, 1511−1514.

(14) Magdesieva, T. V.; Yamamoto, T.; Tryk, D. A.; Fujishima, A. Electrochemical Reduction of CO_2 with Transition Metal Phthalocyanine and Porphyrin Complexes Supported on Activated Carbon Fibers. *J. Electrochem. Soc.* **2002**, *149*, D89−D95.

(15) Lefevre, M.; Proietti, E.; Jaouen, F.; Dodelet, J. P. Iron-Based Catalysts with Improved Oxygen Reduction Activity in Polymer Electrolyte Fuel Cells. *Science* **2009**, *324*, 71−74.

(16) Tylus, U.; Jia, Q. Y.; Strickland, K.; Ramaswamy, N.; Serov, A.; Atanassov, P.; Mukerjee, S. Elucidating Oxygen Reduction Active Sites in Pyrolyzed Metal-Nitrogen Coordinated Non-Precious-Metal Electrocatalyst Systems. *J. Phys. Chem. C* **2014**, *118*, 8999−9008.

(17) Lee, D. H.; Lee, W. J.; Lee, W. J.; Kim, S. O.; Kim, Y. H. Theory, Synthesis, and Oxygen Reduction Catalysis of Fe-Porphyrin-Like Carbon Nanotube. *Phys. Rev. Lett.* **2011**, *106*, 175502.

(18) Yang, J. B.; Liu, D. J.; Kariuki, N. N.; Chen, L. X. Aligned Carbon Nanotubes with Built-in FeN_4 Active Sites for Electrocatalytic Reduction of Oxygen. *Chem. Commun.* **2008**, 329−331.

(19) Zhang, S.; Kang, P.; Ubnoske, S.; Brennaman, M. K.; Song, N.; House, R. L.; Glass, J. T.; Meyer, T. J. Polyethylenimine-Enhanced Electrocatalytic Reduction of CO_2 to Formate at Nitrogen-Doped Carbon Nanomaterials. *J. Am. Chem. Soc.* **2014**, *136*, 7845−7848.

(20) Zhu, W. L.; Michalsky, R.; Metin, O.; Lv, H. F.; Guo, S. J.; Wright, C. J.; Sun, X. L.; Peterson, A. A.; Sun, S. H. Monodisperse Au Nanoparticles for Selective Electrocatalytic Reduction of Co2 to Co. *J. Am. Chem. Soc.* **2013**, *135*, 16833−16836.

(21) Lu, Q.; Rosen, J.; Zhou, Y.; Hutchings, G. S.; Kimmel, Y. C.; Chen, J. G. G.; Jiao, F. A Selective and Efficient Electrocatalyst for Carbon Dioxide Reduction. *Nat. Commun.* **2014**, *5*, 1−6.

(22) Kortlever, R.; Peters, I.; Koper, S.; Koper, M. T. M. Electrochemical Co2 Reduction to Formic Acid at Low Overpotential and with High Faradaic Efficiency on Carbon-Supported Bimetallic Pd−Pt Nanoparticles. *ACS Catal.* **2015**, *5*, 3916−3923.

(23) Karamad, M.; Tripkovic, V.; Rossmeisl, J. Intermetallic Alloys as CO Electroreduction Catalysts-Role of Isolated Active Sites. *ACS Catal.* **2014**, *4*, 2268−2273.

(24) Tripkovic, V.; Vanin, M.; Karamad, M.; Björketun, M. E.; Jacobsen, K. W.; Thygesen, K. S.; Rossmeisl, J. Electrochemical CO_2 and CO Reduction on Metal-Functionalized Porphyrin-Like Graphene. *J. Phys. Chem. C* **2013**, *117*, 9187−9195.

(25) Kresse, G.; Hafner, J. *ab*-Initio Molecular-Dynamics Simulation of the Liquid-Metal Amorphous-Semiconductor Transition in

DOI: 10.1021/acs.jpcc.5b05518
J. Phys. Chem. C 2015, 119, 21345−21352

Germanium. *Phys. Rev. B: Condens. Matter Mater. Phys.* **1994**, *49*, 14251−14269.
(26) Kresse, G.; Hafner, J. *ab*-initio Molecular-Dynamics for Liquid-Metals. *Phys. Rev. B: Condens. Matter Mater. Phys.* **1993**, *47*, 558−561.
(27) Kresse, G.; Furthmuller, J. Efficient Iterative Schemes for *ab Initio* Total-Energy Calculations Using a Plane-Wave Basis Set. *Phys. Rev. B: Condens. Matter Mater. Phys.* **1996**, *54*, 11169−11186.
(28) Kresse, G.; Furthmuller, J. Efficiency of Ab-Initio Total Energy Calculations for Metals and Semiconductors Using a Plane-Wave Basis Set. *Comput. Mater. Sci.* **1996**, *6*, 15−50.
(29) Kresse, G.; Joubert, D. From Ultrasoft Pseudopotentials to the Projector Augmented-Wave Method. *Phys. Rev. B: Condens. Matter Mater. Phys.* **1999**, *59*, 1758−1775.
(30) Blochl, P. E. Projector Augmented-Wave Method. *Phys. Rev. B: Condens. Matter Mater. Phys.* **1994**, *50*, 17953−17979.
(31) Perdew, J. P.; Burke, K.; Ernzerhof, M. Generalized Gradient Approximation Made Simple. *Phys. Rev. Lett.* **1996**, *77*, 3865−3868.
(32) Fishman, M.; Zhuang, H. L. L.; Mathew, K.; Dirschka, W.; Hennig, R. G. Accuracy of Exchange-Correlation Functionals and Effect of Solvation on the Surface Energy of Copper. *Phys. Rev. B: Condens. Matter Mater. Phys.* **2013**, *87*, 245402.
(33) Mathew, K.; Sundararaman, R.; Letchworth-Weaver, K.; Arias, T. A.; Hennig, R. G. Implicit Solvation Model for Density-Functional Study of Nanocrystal Surfaces and Reaction Pathways. *J. Chem. Phys.* **2014**, *140*, 084106.
(34) Nørskov, J. K.; Rossmeisl, J.; Logadottir, A.; Lindqvist, L.; Kitchin, J. R.; Bligaard, T.; Jonsson, H. Origin of the Overpotential for Oxygen Reduction at a Fuel-Cell Cathode. *J. Phys. Chem. B* **2004**, *108*, 17886−17892.
(35) Janik, M. J.; Taylor, C. D.; Neurock, M. First-Principles Analysis of the Initial Electroreduction Steps of Oxygen over Pt(111). *J. Electrochem. Soc.* **2009**, *156*, B126−B135.
(36) Tripkovic, V.; Skulason, E.; Siahrostami, S.; Nørskov, J. K.; Rossmeisl, J. The Oxygen Reduction Reaction Mechanism on Pt(111) from Density Functional Theory Calculations. *Electrochim. Acta* **2010**, *55*, 7975−7981.
(37) Cheng, M. J.; Head-Gordon, M.; Bell, A. T. How to Chemically Tailor Metal-Porphyrin-Like Active Sites on Carbon Nanotubes and Graphene for Minimal Overpotential in the Electrochemical Oxygen Evolution and Oxygen Reduction Reactions. *J. Phys. Chem. C* **2014**, *118*, 29482−29491.
(38) Cao, R.; Thapa, R.; Kim, H.; Xu, X.; Kim, M. G.; Li, Q.; Park, N.; Liu, M. L.; Cho, J. Promotion of Oxygen Reduction by a Bio-Inspired Tethered Iron Phthalocyanine Carbon Nanotube-Based Catalyst. *Nat. Commun.* **2013**, *4*, 2076.
(39) Chlistunoff, J.; Sansiñena, J. M. Effects of Axial Coordination of the Metal Center on the Activity of Iron Tetraphenylporphyrin as a Nonprecious Catalyst for Oxygen Reduction. *J. Phys. Chem. C* **2014**, *118*, 19139−19149.
(40) Jemine, X.; Goffart, J.; Berthet, J. C.; Ephritikhine, M. Absolute Uranium Ligand Bond-Disruption Enthalpies of [U(C_5H_4R)3x] Complexes (X = I or H, R = Bu(T) or SiMe3). *J. Chem. Soc., Dalton Trans.* **1992**, 2439−2440.
(41) Jones, M. B.; Gaunt, A. J. Recent Developments in Synthesis and Structural Chemistry of Nonaqueous Actinide Complexes. *Chem. Rev.* **2013**, *113*, 1137−1198.
(42) Woodruff, D. N.; Winpenny, R. E. P.; Layfield, R. A. Lanthanide Single-Molecule Magnets. *Chem. Rev.* **2013**, *113*, 5110−5148.
(43) Alexander, V. Design and Synthesis of Macrocyclic Ligands and Their Complexes of Lanthanides and Actinides. *Chem. Rev.* **1995**, *95*, 273−342.
(44) Zuend, S. J.; Lam, O. P.; Heinemann, F. W.; Meyer, K. Carbon Dioxide Insertion into Uranium-Activated Dicarbonyl Complexes. *Angew. Chem., Int. Ed.* **2011**, *50*, 10626−10630.
(45) Andrez, J.; Pecaut, J.; Bayle, P. A.; Mazzanti, M. Tuning Lanthanide Reactivity Towards Small Molecules with Electron-Rich Siloxide Ligands. *Angew. Chem., Int. Ed.* **2014**, *53*, 10448−10452.
(46) Mansell, S. M.; Kaltsoyannis, N.; Arnold, P. L. Small Molecule Activation by Uranium Tris(Aryloxides): Experimental and Computational Studies of Binding of N_2, Coupling of CO, and Deoxygenation Insertion of CO_2 under Ambient Conditions. *J. Am. Chem. Soc.* **2011**, *133*, 9036−9051.
(47) Evans, W. J.; Rego, D. B.; Ziller, J. W.; DiPasquale, A. G.; Rheingold, A. L. Facile Insertion of CO_2 into Tetra- and Pentamethylcyclopentadienyl Lanthanide Moieties to Form ($C_5Me_4RCO_2$)(−) Carboxylate Ligands (R = H, Me). *Organometallics* **2007**, *26*, 4737−4745.
(48) Lim, H. K.; Shin, H.; Goddard, W. A.; Hwang, Y. J.; Min, B. K.; Kim, H. Embedding Covalency into Metal Catalysts for Efficient Electrochemical Conversion of CO_2. *J. Am. Chem. Soc.* **2014**, *136*, 11355−11361.
(49) Appel, A. M.; et al. Frontiers, Opportunities, and Challenges in Biochemical and Chemical Catalysis of CO_2 Fixation. *Chem. Rev.* **2013**, *113*, 6621−6658.
(50) Boddien, A.; Gartner, F.; Federsel, C.; Sponholz, P.; Mellmann, D.; Jackstell, R.; Junge, H.; Beller, M. CO_2-"Neutral" Hydrogen Storage Based on Bicarbonates and Formates. *Angew. Chem., Int. Ed.* **2011**, *50*, 6411−6414.
(51) Grasemann, M.; Laurenczy, G. Formic Acid as a Hydrogen Source - Recent Developments and Future Trends. *Energy Environ. Sci.* **2012**, *5*, 8171−8181.
(52) Boddien, A.; Junge, H. Catalysis Acidic Ideas for Hydrogen Storage. *Nat. Nanotechnol.* **2011**, *6*, 265−266.
(53) Hull, J. F.; Himeda, Y.; Wang, W. H.; Hashiguchi, B.; Periana, R.; Szalda, D. J.; Muckerman, J. T.; Fujita, E. Reversible Hydrogen Storage Using CO_2 and a Proton-Switchable Iridium Catalyst in Aqueous Media under Mild Temperatures and Pressures. *Nat. Chem.* **2012**, *4*, 383−388.
(54) Loges, B.; Boddien, A.; Gartner, F.; Junge, H.; Beller, M. Catalytic Generation of Hydrogen from Formic Acid and Its Derivatives: Useful Hydrogen Storage Materials. *Top. Catal.* **2010**, *53*, 902−914.
(55) Tedsree, K.; Li, T.; Jones, S.; Chan, C. W. A.; Yu, K. M. K.; Bagot, P. A. J.; Marquis, E. A.; Smith, G. D. W.; Tsang, S. C. E. Hydrogen Production from Formic Acid Decomposition at Room Temperature Using a Ag-Pd Core-Shell Nanocatalyst. *Nat. Nanotechnol.* **2011**, *6*, 302−307.
(56) Yu, W. Y.; Mullen, G. M.; Flaherty, D. W.; Mullins, C. B. Selective Hydrogen Production from Formic Acid Decomposition on Pd-Au Bimetallic Surfaces. *J. Am. Chem. Soc.* **2014**, *136*, 11070−11078.
(57) Agarwal, A. S.; Zhai, Y. M.; Hill, D.; Sridhar, N. The Electrochemical Reduction of Carbon Dioxide to Formate/Formic Acid: Engineering and Economic Feasibility. *ChemSusChem* **2011**, *4*, 1301−1310.
(58) Yu, X. W.; Pickup, P. G. Recent Advances in Direct Formic Acid Fuel Cells (DFAFC). *J. Power Sources* **2008**, *182*, 124−132.

DOI: 10.1021/acs.jpcc.5b05518
J. Phys. Chem. C 2015, 119, 21345−21352